Post-plasma catalytic removal of methanol over Mn-Ce catalysts in an atmospheric dielectric barrier discharge

Xinbo Zhu[1, 2§], Shiyun Liu[2§], Yuxiang Cai[1], Xiang Gao[1 *], Jinsong Zhou, Chenghang Zheng[1], Xin Tu[2 *]

[1] State Key Laboratory of Clean Energy Utilization, Department of Energy Engineering, Zhejiang University, Hangzhou 310027, Zhejiang Province, China

[2] Department of Electrical Engineering and Electronics, University of Liverpool, Liverpool, L69 3GJ, UK

§ - equal contribution

Corresponding authors

*** Dr. Xin Tu**

Department of Electrical Engineering and Electronics,

University of Liverpool,

Liverpool, L69 3GJ, UK

E-mail: xin.tu@liverpool.ac.uk

Tel: +44-1517944513

*** Prof. Xiang Gao**

State Key Laboratory of Clean Energy Utilization, Zhejiang University,

Hangzhou 310027, Zhejiang Province, China

E-mail: xgao1@zju.edu.cn

Abstract:

A post-plasma catalysis system has been developed for the removal of methanol over Mn-Ce oxide catalysts with different Mn/Ce molar ratios at low temperatures. The $Mn_{50}Ce_{50}$ oxide catalyst (Mn/Ce=1:1) shows the best performance in terms of methanol removal efficiency and energy efficiency of the plasma-catalytic process. The maximum methanol removal efficiency of 99.8% can be achieved at a discharge power of 16.5 W, while the highest energy efficiency of the plasma-catalytic process is 47.5 g/kWh at 1.9 W. The combination of plasma and Mn-Ce catalysts significantly reduces the formation of major by-products (methane, formaldehyde and formic acid) based on the Fourier transform infrared spectra. Possible reaction mechanisms and pathways of the post-plasma catalytic removal of methanol are also proposed. A three-layer back propagation artificial neural network (ANN) model has been developed to get a better understanding of the roles of different process parameters on methanol removal efficiency and energy efficiency in the post-plasma catalytic process. The predicted data from the ANN model show a good agreement with the experimental results. Catalyst composition (i.e. Mn/Ce ratio) is found to be the most important factor affecting methanol removal efficiency with a relative importance of 31.53%, while the discharge power is the most influential parameter for energy efficiency with a relative weight of 30.40%. These results indicate that the well-trained ANN model provides an alternative approach for accurate and fast prediction of the plasma-catalytic chemical reactions.

Keywords: Plasma-catalysis, dielectric barrier discharge, methanol removal, artificial neural network, environmental clean-up

1. Introduction

Volatile organic compounds (VOCs) emitted by human activities are one of the major sources for the formation of photochemical smog and haze [1]. Due to their negative effects on both the environment and human health, air pollution of VOCs has become a global environmental issue. However, conventional technologies, such as adsorption, absorption, thermal catalytic oxidation and combustion, are not cost-effective when dealing with dilute VOCs in high volume gas streams [2].

Over the past decades, non-thermal plasma (NTP) technology has been considered as an attractive and promising alternative for the removal of a wide range of VOCs at atmospheric pressure and low temperatures [3]. A hybrid technology combining the use of non-thermal plasma with catalysis, known as "plasma-catalysis", has gained increased attention to overcome the disadvantages of NTP processes such as the formation of hazardous by-products. The synergistic effect resulting from the interactions between the plasma and catalysts can lower the operating temperature of catalytic reactions, improve the decomposition of environmental pollutants and change the selectivity of the plasma process to minimize unwanted by-products, as well as enhance the energy efficiency of the plasma process [4].

Plasma-catalysis technology has been demonstrated to be promising for the removal of a wide range of dilute VOCs in waste gas streams [5]-[11]. Mn-based catalysts have been widely used in plasma-catalytic processes especially in the post-plasma catalysis configuration due to their ability to efficiently decompose ozone at ambient temperature. This leads to the formation of reactive oxygen species for further oxidation of residual pollutants in the effluent, and consequently increases the removal efficiency of VOCs. Jarrige et al. reported that the combination of a pulsed corona discharge with MnO_x-Al_2O_3 post-treatment improved the removal efficiency of propane (200 ppm) by over 40% at a specific energy density (SED) of 200 J/L, while the yield of CO_2 was 15% higher than that using plasma alone [12]. Li et al. found that the removal of acetaldehyde was enhanced by over 20% in the presence of MnO_2/γ-Al_2O_3 compared to that using plasma alone at the SED of 8 J/L, while α-MnO_2/γ-Al_2O_3 catalyst exhibited the best activity among all tested catalysts [13]. Cerium oxide (CeO_2) is

known as a good promoter for Mn-based catalysts due to its oxygen storage capacity (OSC). Mn-Ce oxides have shown excellent activity in thermal-catalytic processes such as selective catalytic reduction of NO_x and catalytic oxidation of VOCs [14][15]. The addition of Ce to MnO_x can enhance catalyst performance due to the increased surface area and Mn dispersion, and higher reducibility with the involvement of surface oxygen species in reactions [16][17]. However, very limited work has been carried out using Mn-Ce catalysts in plasma-catalytic oxidation of VOCs [18]. In addition, previous works were mainly focused on the plasma-catalytic removal of low concentration (10-1000 ppm) gas pollutants in high volume waste streams, while the destruction of VOCs with higher concentration (e.g. several thousand ppm) using plasma-catalysis is more challenging and has attracted considerable interest from industry, especially the industry in China due to serious environmental pollutions. Removal of dilute methanol of either low or high concentration over Mn-Ce catalysts in a plasma-catalysis system has not been reported before.

Plasma-catalysis is a complex process and the reaction performance of the process is controlled by a wide range of process parameters [18]-[22]. Most of the previous work has mainly focused on experimental investigations to evaluate the effect of individual process parameters on the plasma reaction performance [7][23], while a fundamental understanding of the contribution of each factor and the interaction of different factors to plasma-catalytic reactions is almost nonexistent, making it difficult to optimize the process parameters and predict the plasma reaction performance theoretically. Numerical modeling of plasma-assisted VOC decomposition has been proposed to solve this problem [24][25]. Aerts et al. developed a global kinetic 0D model which consisted of 113 species (electrons, atoms, ions and molecules) and 1639 reactions, even without a catalyst to investigate the removal of ethylene in an air dielectric barrier discharge reactor [26][27]. However, although model calculations can be fast, depending on the type of model, the development of a comprehensive model takes time, and is thus not always desirable for the fast and cost-effective prediction and optimization of highly complex and non-linear plasma processes. A recent review article has pointed out that it is still a

challenge to develop a comprehensive model involving plasma physics, plasma chemistry and surface science to deal with the entire plasma-catalytic process [25].

Artificial neural networks (ANNs) are considered as a promising tool for process modeling and optimization. Due to their ability of self-learning, modeling and prediction, ANNs are able to reproduce a mapping of the input and output variables based on limited experimental samples with sufficient process units (neurons). As a data-driven model, ANNs are able to predict the performance of complex processes, which are often not represented by mathematical formulas. More importantly, less time is needed for the training and optimization of the ANN model [28]. The developed and well-trained ANN model can precisely predict the output performance of complex nonlinear systems as a function of suitable input variables. Such a mapping can subsequently be used to predict desired outputs as a function of suitable input variables, even out of the trained regions. For example, multiple-layer ANNs have been used for forecasting a wide range of industrial processes such as the prediction of electrical demand for the national grid. However, there are very few studies on the application of ANNs in the simulation and prediction of plasma chemical reactions, especially plasma-catalytic processes [29][30].

In this work, methanol is chosen as a model environmental pollutant since it is a toxic and volatile alcohol that has been widely used industrially as a solvent, pesticide, and alternative fuel source. Inhalation or ingestion of methanol may result in blurred vision, headache, dizziness, and nausea. A post-plasma catalytic process has been developed for the removal of dilute methanol over the Mn-Ce catalysts with different Mn/Ce molar ratios. The effect of a wide range of plasma process parameters including the discharge power, Mn percentage, gas flow rate and initial methanol concentration on the reaction performance has been investigated in terms of methanol removal efficiency and energy efficiency of the plasma-catalytic process. Possible reaction mechanisms and pathways involved in the plasma-catalytic process are discussed and proposed based on the identified gas products. A well-trained back propagation (BP) artificial neural network model has been developed for the modeling of the post-plasma catalytic process to get new insights into the effect

and relative importance of different plasma process parameters on the plasma reaction performance and to predict the post-plasma catalytic processing of methanol in terms of methanol removal efficiency and energy efficiency.

2. Materials and methods

2.1 Experimental Setup

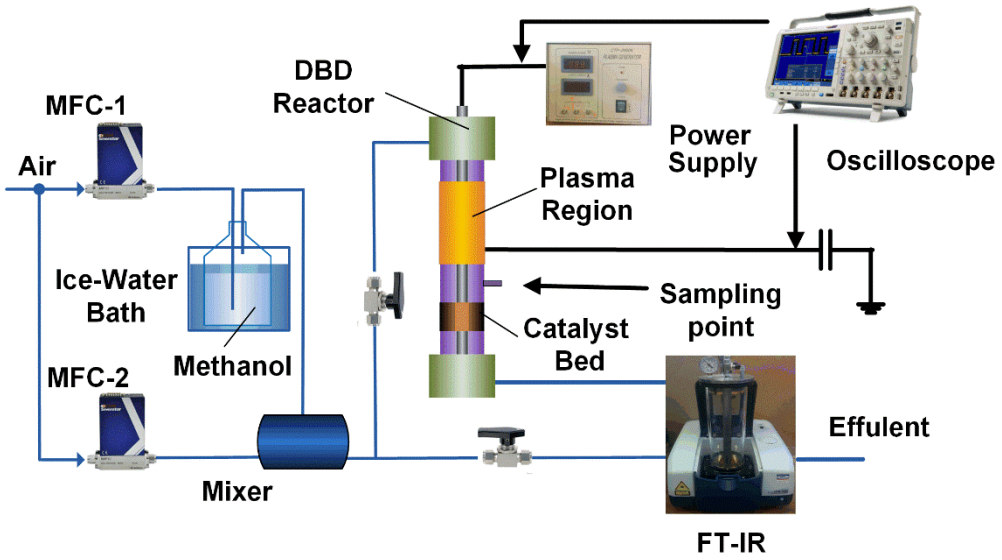

Fig. 1. Schematic diagram of the experimental setup

The experiment was carried out in a coaxial dielectric barrier discharge (DBD) reactor, as shown in Fig. 1. A 60 mm-long aluminum foil (ground electrode) was wrapped over a quartz tube with an inner diameter of 8 mm and wall thickness of 1 mm. A stainless steel rod with an outer diameter of 4 mm was placed in the quartz tube and acted as a high voltage electrode. As a result, the discharge volume was 2.26 cm^3, while the residence time of the mixture gas was 0.14 s at an air flow rate of 1 L/min. The reactor was connected to an AC power supply with a maximum peak voltage of 30 kV and frequency of 10 kHz. Air was used as carrier gas (BOC, zero grade, moisture less than 5 ppm), while methanol (Alfa Aesar) was introduced into the DBD reactor by passing a dry air flow (10 mL/min) through a bubbler kept in a thermostatic ice-water bath (0 ^oC). High concentration of methanol (1500-4500 ppm) was chosen for the modeling of the ANN. All gas streams were premixed

prior to the DBD reactor. An online power measurement system was used to monitor and control the discharge power (P) of the DBD reactor in real time. The discharge power of the DBD was calculated using Lissajous method [31]. The gas temperature in the center of the discharge area was measured by using a fiber optical thermometer (Omega, FOB102). The maximum gas temperature in the DBD was less than 150 ^{o}C.

2.2 Catalysts preparation and characterizations

Mn-Ce oxide catalysts with different Mn contents were synthesized using the citric-acid method [8]. Desired amount of manganese nitrate, ceria nitrate and citric acid (Alfa Aesar) were dissolved in deionized water. The stoichiometric ratio of citric acid to metal salts was 1.5. The obtained solution was vigorously stirred at room temperature for 2 h. After that, the solution was stirred in a water bath at 80 °C to get wet gel, followed by further drying overnight at 110 °C and calcination at 500 °C for 5 h. Pure manganese oxide and ceria oxide were prepared in the same way. All catalysts were denoted as Mn_xCe_{100-x}, where x is the molar percentage (%) of Mn. All the samples were sieved to 35-60 meshes. The catalyst pellets (100 mg) were packed into the discharge gap at 50 mm downstream of the plasma zone, as a post-plasma catalysis configuration. There is no extra heating for the catalyst bed.

2.3 Gas analysis

Gas compositions before and after the catalyst bed were analyzed using a Fourier transform infra-red (FTIR) spectrometer (Jasco FTIR-4200) with a resolution of 2 cm^{-1}. The FTIR spectrometer was equipped with a 1-16 m variable gas cell (PIKE Technologies), while the effective path length used in this study was 5.3 m. Measurements were carried out after running the plasma reaction for about 40 minutes, when a steady-state was reached. All experimental data were obtained by averaging 128 scans and repeating 3 times, with the average value of the three measurements being presented.

The removal efficiency (RE) of methanol (CH_3OH) is defined as:

$$\eta_{CH_3OH} = \frac{c_{in} - c_{out}}{c_{in}} \times 100\% \quad (2)$$

where c_{in} and c_{out} are the methanol concentrations in the untreated gas and effluent, respectively.

The energy efficiency (EE) for the removal of methanol in the plasma-catalytic process can be defined as:

$$EE \text{ (g/kWh)} = \frac{M_{CH_3OH} \cdot \eta_{CH_3OH} \cdot c_{in} \cdot Q}{P \cdot V_m} \times 3.6 \times 10^6 \quad (3)$$

where M_{CH_3OH} is the molecular weight of methanol (*g/mol*), *Q* is the total gas flow rate (*L/min*), *P* is the discharge power (*W*), and V_m is the molar volume (*L/mol*).

2.4 Artificial neural network

A three-layer (input, hidden and output layers) ANN model has been developed for the modeling and prediction of the plasma-catalytic removal of methanol by using MATLAB neural network toolbox. Four key process parameters: discharge power, total gas flow rate, initial methanol concentration and catalyst composition (Mn percentage) are identified as the input variables of the ANN, while methanol removal efficiency and energy efficiency of the process are used as the output variables. Therefore, the input and output layer consist of 4 and 2 neurons, respectively.

The experimental samples were split into two groups: an input group (X) and a target output group (T). 70 sets of experimental data were randomly divided into training (70%), validation (~15.7%) and test (~14.3%) groups; each contains 49, 11 and 10 data sets, respectively. The ANN model learns by manipulating the connection weights. The weights are adjusted to minimize the mean square error (MSE) and standard deviation error (SDE). Each network topology was trained for 20 times to counteract the effect of random weights initialization of the network.

BP training algorithm is one of the most popular supervised learning algorithms for the training of feed-forward ANN [30]. The combination of Levenberg–Marquardt (LM) training algorithm with

a TANSIG transfer function at both the hidden and output layers (TT) is chosen for the ANN due to its best accuracy among the tested cases using orthogonal experiments (see Table S1 in Supporting Information).

The optimal neuron number at the hidden layer was determined to be 12 as the minimum training error was obtained (see Fig. S1 in Supporting Information). The optimized configuration of the ANN for plasma-catalytic methanol decomposition is shown in Fig. 2. Finally, the validation of ANN model shows a perfect agreement between the predicted and experimental results with a correlation coefficient (R^2) of 0.99662 (Fig. S2 in Supporting Information).

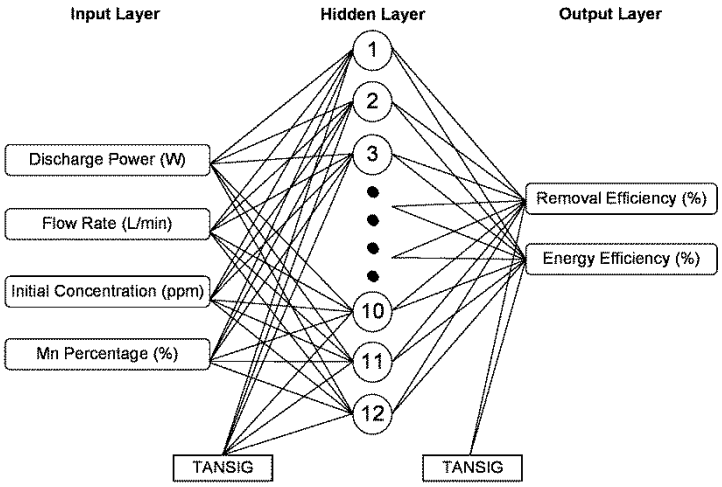

Fig. 2. Optimized three-layer ANN model

3. Results and discussion

3.1 Catalyst characterization

The material characteristics of the fresh catalyst samples are listed in Table 1. Compared to the specific surface area (S_{BET}) of MnO_x (15.0 m^2 g^{-1}) and CeO_2 (23.8 m^2 g^{-1}), the combination of Mn and Ce species resulted in the formation of a large specific surface area (46.5 m^2 g^{-1} to 88.9 m^2 g^{-1}) of the Mn-Ce catalysts, which could provide more active sites on the catalyst surface for the oxidation

of methanol. The $Mn_{50}Ce_{50}$ catalyst has the highest S_{BET} of 88.9 m^2 g^{-1}, while further increasing the amount of Mn or Ce resulted in a decrease of the S_{BET} of the Mn-Ce catalysts.

Fig. 3 shows the XRD patterns of the fresh catalysts. For the MnO_x catalyst, typical diffraction peaks of Mn_2O_3 phase (JCPDS 78-0390) can be clearly observed. The XRD spectra of the CeO_2 and Mn-Ce catalysts show a typical diffraction pattern of cubic fluorite-type oxide structure (JCPDS 34-0394). No obvious peaks of manganese oxides are observed in the $Mn_{50}Ce_{50}$ and $Mn_{25}Ce_{75}$ samples, which might be attributed to the effective dispersion of manganese oxides on the catalyst surface or the incorporation of Mn species into CeO_2 lattice. Further increasing the Mn content leads to the formation of bulk Mn_3O_4 (JCPDS 024-0734) and Mn_2O_3, which can be confirmed by the diffraction peaks in the XRD pattern of the $Mn_{75}Ce_{25}$ catalyst. Moreover, the introduction of Mn into CeO_2 results in broad diffraction peaks, indicating the formation of the amorphous structure and smaller crystalline size of the catalysts, which favours the removal of methanol.

Table 1. Material properties of Mn-Ce catalysts

Sample	Specific surface area (m^2 g^{-1})	Total pore volume (cm^3 g^{-1})	Average pore size (nm)
MnO_x	15.0	0.049	8.35
$Mn_{75}Ce_{25}$	71.0	0.144	5.99
$Mn_{50}Ce_{50}$	88.9	0.222	4.76
$Mn_{25}Ce_{75}$	46.5	0.201	6.17
CeO_2	23.8	0.106	7.62

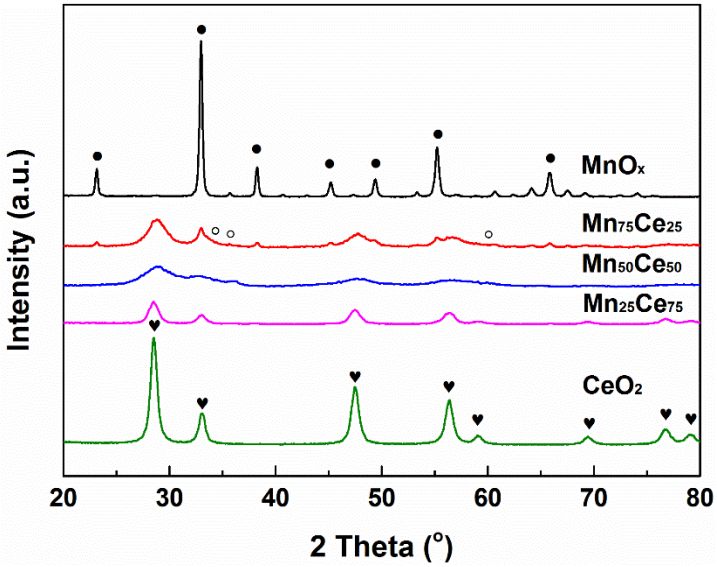

Fig. 3. XRD patterns of Mn-Ce catalysts.

3.2 Plasma-catalytic removal of methanol

3.2.1 Effect of discharge power

Fig. 4 shows a comparison between the experimental and predicted results for the plasma-catalytic removal of methanol over different Mn-Ce catalysts in the discharge power range of 1.9 - 15 W. The simulated results obtained from the ANN model are in good agreement with the experimental data. The discharge power significantly influences the reaction performance of the plasma-catalytic removal of methanol regardless of the catalysts used. Taking the $Mn_{50}Ce_{50}$ catalyst as an example, methanol removal efficiency increases almost linearly from 34.6% to 95.4% with the increase of the discharge power from 1.9 W to 15.0 W, as shown in Fig. 4a. The well-trained ANN model could predict the performance of the plasma-catalysis system under other operating conditions. For example, the predicted methanol removal efficiency at the discharge power of 7.0 W and 16.5 W is 65.4% and 97.8%, respectively. In contrast, increasing the discharge power from 1.9 W to 15.0 W decreases the energy efficiency by a factor of 2.88. In this study, the maximum energy efficiency of 47.5 g/kWh is obtained at the lowest discharge power of 1.9 W (Fig. 4b). These results suggest that a balance between the destruction of pollutants and energy efficiency of the plasma-catalytic process should be considered when developing a cost-effective plasma-catalytic technology.

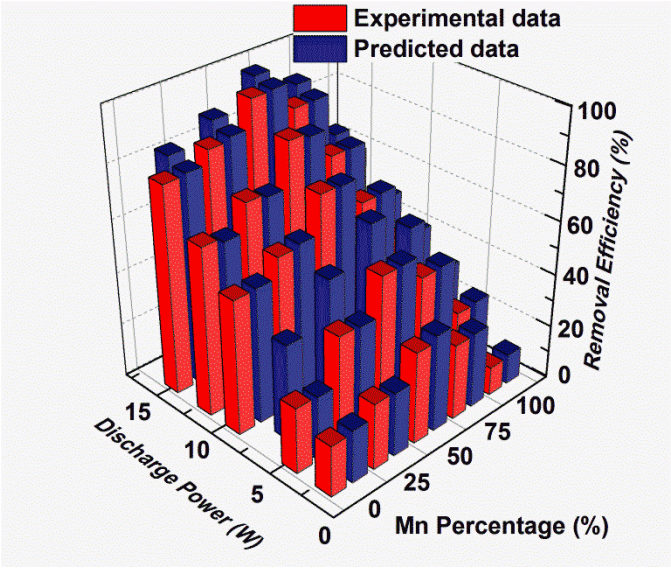

(a)

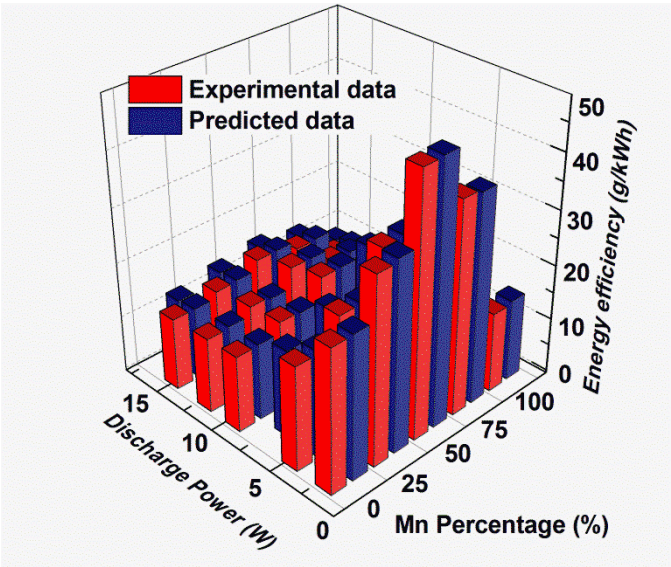

(b)

Fig. 4. Effect of discharge power on the plasma-catalytic removal of methanol over Mn-Ce catalysts: (a) removal efficiency; (b) energy efficiency (*Q*: 1 L/min, *C*: 3000 ppm).

3.2.2 Effect of Mn percentage

Catalyst composition is one of the key factors affecting the plasma-catalytic process of methanol removal. The effect of Mn percentage on methanol removal efficiency and energy efficiency at different discharge powers has also been investigated, as presented in Fig. 4. Both predicted removal

efficiency and energy efficiency are in good agreement with the experimental data inside and outside of the catalyst composition range. In this study, pure MnO_x is the least active catalyst for the plasma removal of methanol followed by pure CeO_2 in the tested discharge power range. The interaction of Mn and Ce species significantly enhances the reaction performances and the activity of Mn-Ce catalysts follow the order of $Mn_{50}Ce_{50}$ > $Mn_{75}Ce_{25}$ > $Mn_{25}Ce_{75}$. This agrees with the properties of the Mn-Ce catalysts given in Table 1 which show that the $Mn_{50}Ce_{50}$ sample has the largest specific surface area. At the discharge power of 9.4 W, the maximum methanol removal efficiency and energy efficiency of the system can be achieved at 73.5% and 20.1 g/kWh, respectively, in the presence of the $Mn_{50}Ce_{50}$ catalyst. Previous work also reported that Mn-Ce oxide catalyst with a molar ratio of 1:1 exhibited the best performance for thermal catalytic oxidation of toluene, ethanol and ethyl acetate [16]. The influence of Mn content on the energy efficiency of the process follows the similar trend as the removal efficiency. These results suggest that the catalyst composition significantly affects the oxidation process in the catalyst bed. Due to the smaller radius of Mn ions (Mn^{2+} = 0.83 Å, Mn^{3+} = 0.65 Å and Ce^{4+} = 0.97 Å), the partial substitution of Ce^{4+} by Mn cations results in the formation of Mn-Ce solid solutions. Meanwhile, Ce^{3+}, oxygen vacancies and unsaturated chemical bonds could be formed on the catalyst surface to maintain the electroneutrality, which contributes to the formation of active O species for oxidation reactions [32]. When the Mn content is lower than 50%, Mn particles are well dispersed on the surface of CeO_2 and facilitate oxygen mobility in the redox cycles, which enhances the reducibility of the Mn-Ce catalysts [33]. The oxygen storage capacity is determined by the redox couple of Ce^{4+}/Ce^{3+}. Further increasing the content of Mn leads to the formation of separated bulk Mn, and the Mn-O-Mn connections would become more abundant, which may inhibit the formation of oxygen vacancies on the catalyst surface [34], and in turn decrease the oxidation capacity of the Mn-rich catalysts (i.e., $Mn_{75}Ce_{25}$ and pure MnO_x). As a result, both removal efficiency and energy efficiency are decreased when using the Mn-rich samples.

3.2.3 Effect of gas flow rate

Fig. 5 shows the effect of the gas flow rate and Mn-Ce catalyst composition on the removal efficiency of methanol and energy efficiency of the plasma-catalytic process. There is a perfect match between the experimental results and predicted data. The removal efficiency of methanol decreases from 99.5% to 73.3% over the tested flow rate range for the $Mn_{50}Ce_{50}$ catalyst. The gas flow rate shows a significant effect on the reaction performance. Increasing the gas flow rate leads to the decrease of the residence time of pollutants in the plasma region, reducing the possibility of the collisions between methanol molecules and reactive species, and consequently decreasing the removal efficiency of methanol. The optimized ANN model predicts the removal efficiency of 89.5% and 69.3% at the gas flow rate of 0.7 and 1.2 L/min, respectively. However, increasing the flow rate leads to a significant enhancement in the energy efficiency of the process even though the removal efficiency is much lower at a high gas flow rate.

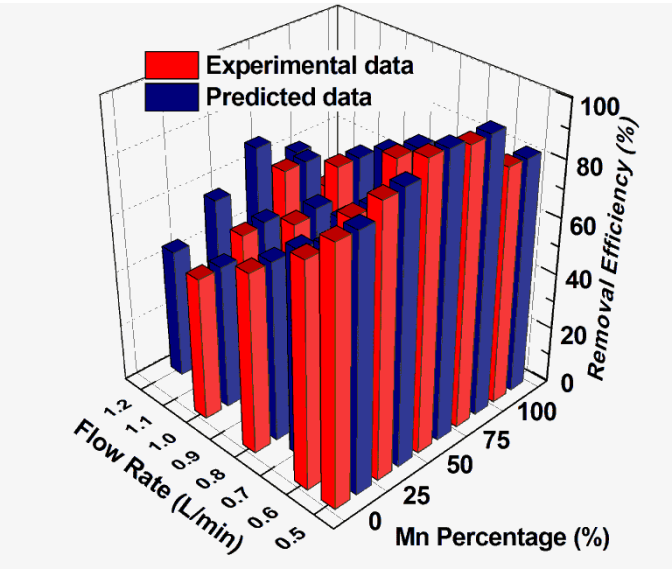

(a)

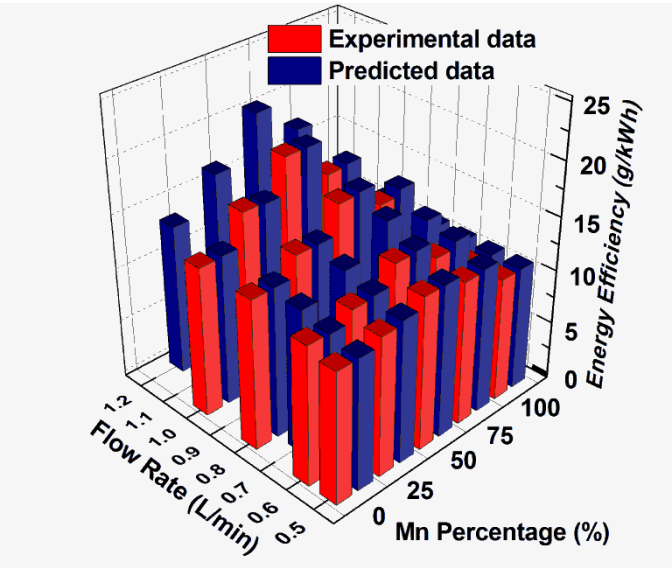

(b)

Fig. 5. Effect of gas flow rate on the plasma-catalytic removal of methanol over Mn-Ce catalysts: (a) removal efficiency; (b) energy efficiency (*P*: 9.4 W, *C*: 3000 ppm).

3.2.4 Effect of initial concentration of methanol

The influence of the initial methanol concentration on the plasma-catalytic removal of methanol over different Mn-Ce catalysts is shown in Fig. 6a. The experimental results are well matched by the ANN simulation. It is clear that the removal efficiency of methanol increases with decreasing initial methanol concentration in the gas flow regardless of the catalysts used. For the $Mn_{50}Ce_{50}$ catalyst, the experimental removal efficiency decreases from 82.7% to 63.3% when the initial concentration of methanol increases from 1500 ppm to 4500 ppm. For a given plasma-catalytic system, the number density of plasma-generated reactive species and active sites could be similar at a same working condition. At this point, only limited number of reactive species and active sites are available for the oxidation of methanol molecules at higher initial concentration, which subsequently reduces the removal efficiency. In contrast, the energy efficiency of the plasma-catalytic process changes from 11.3 g/kWh to 26.0 g/kWh as the concentration of methanol rises from 1500 ppm to 4500 ppm (Fig. 6b). Note that the energy efficiency at 4500 ppm is only 2.3 times of that at 1500 ppm, which is in

line with the results of reduced removal efficiency at high initial concentration. The ANN model predicts that the energy efficiency of the process increases to 27.3 g/kWh at an initial concentration of methanol of 5500 ppm.

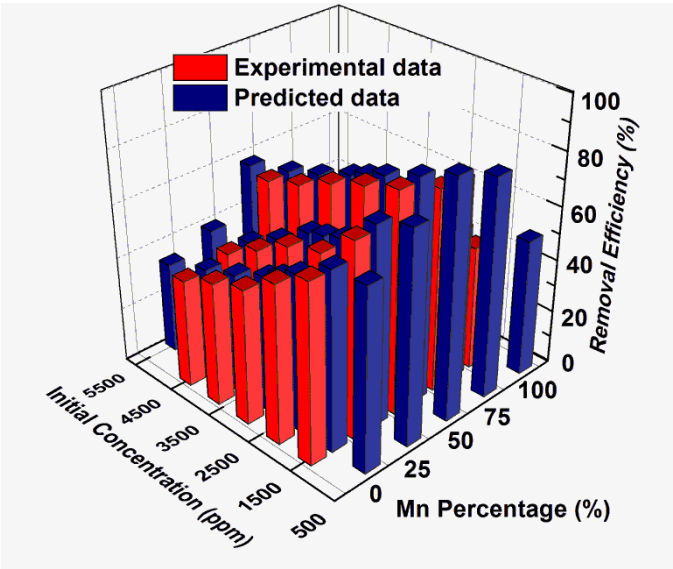

(a)

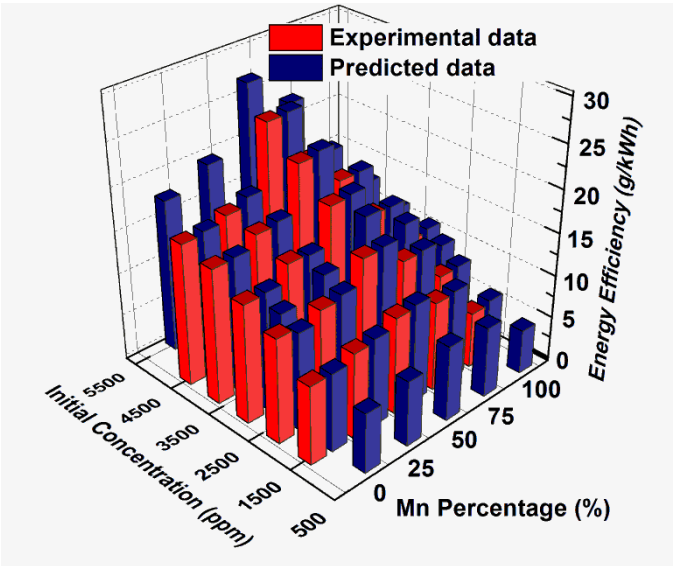

(b)

Fig. 6. Effect of initial concentration of methanol on the plasma-catalytic process: (a) removal efficiency; (b) energy efficiency (*P*: 9.4 W, *Q*: 1 L/min).

3.3 Contribution of different process parameters

Net weight matrix and Garson equation were used in this work to evaluate the relative importance of each process parameter on the plasma chemical reactions [35]. The weight matrix produced by the well-trained ANN model is listed in Table S2 in the Supporting Information, while the calculated relative importance of each process parameter is plotted in Fig. 7. Both gas flow rate and catalyst composition (Mn percentage) show a significant impact on the removal efficiency of methanol with a relative weight of ~31%, while the initial concentration of methanol plays a very weak role in the plasma-catalytic abatement of methanol, which suggests that the plasma system is suitable for the removal of methanol with a wide range of concentration. The discharge power is found to be the most important factor affecting the energy efficiency of the process, while the relative importance of other process parameters on the energy efficiency is similar, ranging from 20.99% to 24.62%.

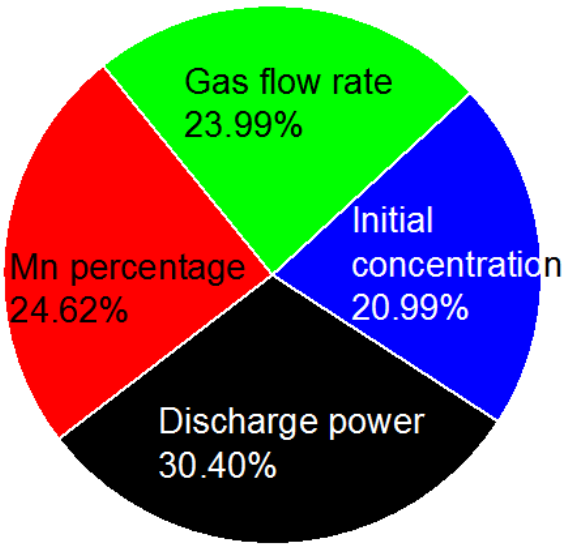

(a)

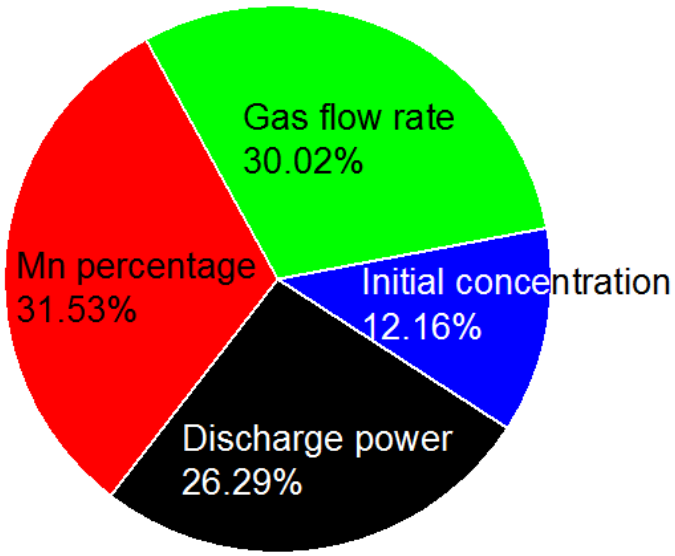

(b)

Fig. 7. Relative importance (%) of processing parameters on plasma-catalytic removal of methanol: (a) removal efficiency; (b) energy efficiency.

3.4 Reaction mechanisms and pathways

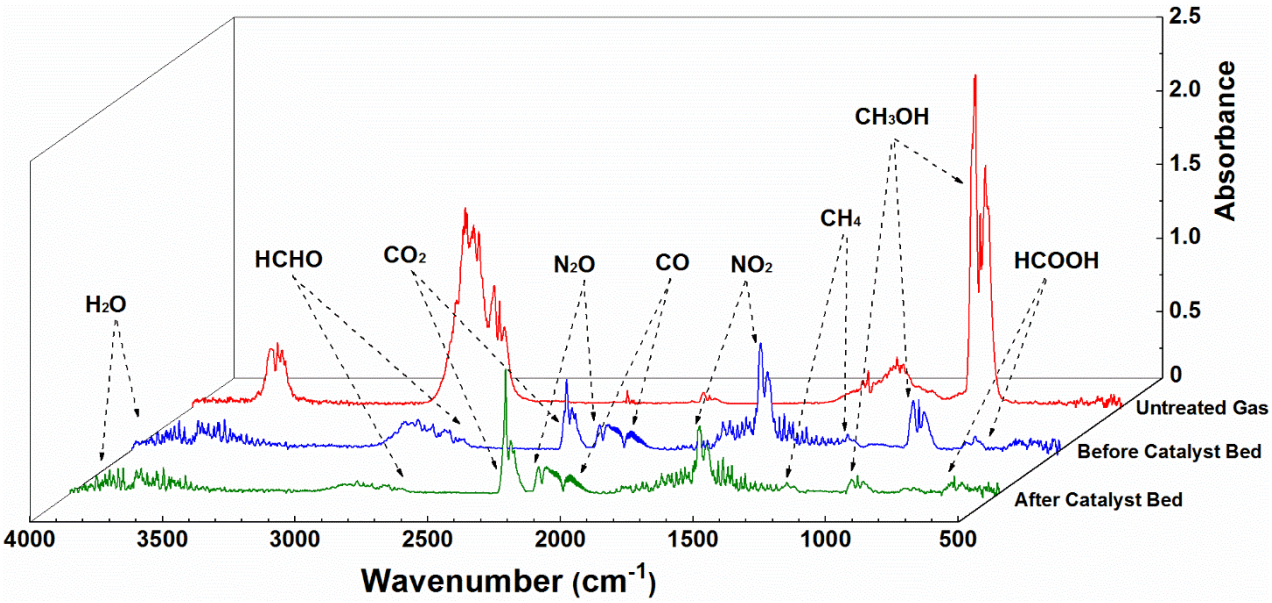

Fig. 8. FTIR spectra of plasma-catalytic removal of methanol over $Mn_{50}Ce_{50}$ catalyst (*P*: 15.0 W, *Q*: 1 L/min, *C*: 3000 ppm).

Fig. 8 shows the distribution of the gas products in the plasma-catalytic removal of methanol over the $Mn_{50}Ce_{50}$ catalyst. The main gas products sampled before the catalyst bed were CO, CO_2

and H_2O, while small amount of CH_4, HCHO, HCOOH, N_2O and NO_2 were also detected. Ozone was not detected since it could be consumed in the oxidation reactions or decomposed by the local heating in the plasma. Similar gas products were detected at the outlet of the plasma reactor after the catalyst bed. However, the intensity of most gas products (CO, CH_4, HCHO, HCOOH, N_2O and NO_2) is significantly decreased except CO_2 and H_2O at the exit of the DBD reactor. These results suggest that the catalyst bed placed after the plasma region plays an important role in the further oxidation of methanol and by-products in this post-plasma catalysis system.

In this post-plasma catalysis system, the catalyst bed is located at 5 cm downstream of the plasma region. Only long-lived species (e.g. methanol and intermediates) can reach the surface of the Mn-Ce catalysts, while most short-lived species such as O and OH could be quenched before reaching the catalyst surface due to their extremely short lifetime and high chemical activity. Thus, the dominant reaction pathways of methanol removal in the two-stage post-plasma catalytic process without extra heating can be identified as two separate steps: plasma reaction in the discharge region and catalytic reaction in the catalyst bed, as shown in Fig. 8.

It is well known that abatement of dilute VOCs in air plasmas is initiated by direct electron impact dissociation of carrier gas (nitrogen and oxygen) to form chemically reactive species such as O, O (^1D), N and N_2 (A) for the stepwise decomposition and oxidation of pollutants and/or intermediates into CO, CO_2, H_2O and other by-products. The formation of these reactive species allows methanol decomposition or oxidation through the following reactions (R1-R5) [36]:

$$CH_3OH + O, O(^1D) \rightarrow CH_2OH\cdot + OH\cdot \quad \text{R1}$$

$$\rightarrow CH_3O\cdot + OH\cdot \quad \text{R2}$$

$$CH_3OH + N, N_2(A) \rightarrow CH_3\cdot + OH\cdot + N, N_2 \quad \text{R3}$$

$$\rightarrow CH_3O\cdot + H + N, N_2 \quad \text{R4}$$

$$\rightarrow CH_2OH\cdot + H + N, N_2 \quad \text{R5}$$

Hydroxyl radicals (OH·) generated from R1, R2 and R3 can also oxidize methanol molecules via [37]:

$$CH_3OH + OH\cdot \rightarrow CH_2OH\cdot + H_2O \quad \text{R6}$$

$$CH_3OH + OH\cdot \rightarrow CH_3O\cdot + H_2O \quad \text{R7}$$

Hamdane et al. reported that the reaction between OH· and CH_3OH is a major pathway for methanol oxidation [37]. However, the effect of electron impact dissociation could be weak or negligible for the dissociation of methanol and other by-products due to the relatively low concentration of these products compared to carrier gas.

CH_3·, CH_2OH· and CH_3O· radicals are the main intermediates of methanol decomposition and oxidation in the air DBD. Previous works also reported that CH_2OH· and CH_3O· are very important radicals for the oxidation of higher hydrocarbons and oxygenates [38]. H-abstractions of CH_2OH· and CH_3O· radicals are also likely to occur via reactions with O, H and OH·, forming CH_2O and HCO·. In the air plasma removal of methanol, CH_3· radicals can be reacted with O and OH to form CH_2· radicals, while some of the CH_3· radicals recombine with H atoms to form CH_4 (Fig. 8). In the presence of oxidative radicals, CH_2· radicals can also be converted to CH_2O and HCO·. Both CH_2O and HCO· can react with O and OH radicals, and form HCOOH [39]. The intermediates and by-products could be further oxidized to form end-products such as CO, CO_2 and H_2O.

In the catalyst bed, methanol and by-products in the gas mixture were adsorbed onto the surface active sites prior to catalytic reactions. It is generally recognized that the oxidation of VOCs on Mn catalysts proceeds via the classical Mars-van Krevelen (MVK) mechanism [40][41]. According to this mechanism, adsorbed VOC molecules were oxidized by active surface oxygen species, while the resultant oxygen vacancies could be replenished by gas phase oxygen. The alternative oxidation and reduction of metal active sites on the catalyst surface in the whole catalytic reaction makes the supply of oxygen species as a rate-determining step [42]. CeO_2 acted as a reservoir for the release and storage of oxygen as a result of the Ce^{4+}/Ce^{3+} redox cycle in the Mn-Ce oxide catalysts. The interactions between Mn and Ce oxides in the Mn-Ce catalysts shows a synergistic effect in oxygen activation,

which enhances the oxygen mobility on the catalysts and accelerates the conversion of oxygen from chemisorbed and lattice oxygen to active oxygen species (O*) on the oxygen vacancies and active metal sites. These processes lead to the deep oxidation of methanol and intermediates by surface active oxygen in the catalyst bed [43]. Finocchio et al. reported that methanol adsorbed onto the surface of Mn-based catalysts can be dissociated and resulted in the break of O-H bonds [44]. The formed $CH_3O\cdot$ can be further dissociated to HCHO and H with the aid of O* [45]. The conversion of HCHO to HCOOH via $HCO\cdot$ on the surface of Mn catalysts was also reported [46]. A fraction of these intermediates and by-products can be further oxidized by O* and finally desorbed as CO and CO_2. The inhibition of NO_x formation in a post-plasma catalysis system are mainly attributed to the oxidation of NO_x to HNO_x and surface adsorbed NO_2^- or NO_3^- cations [10].

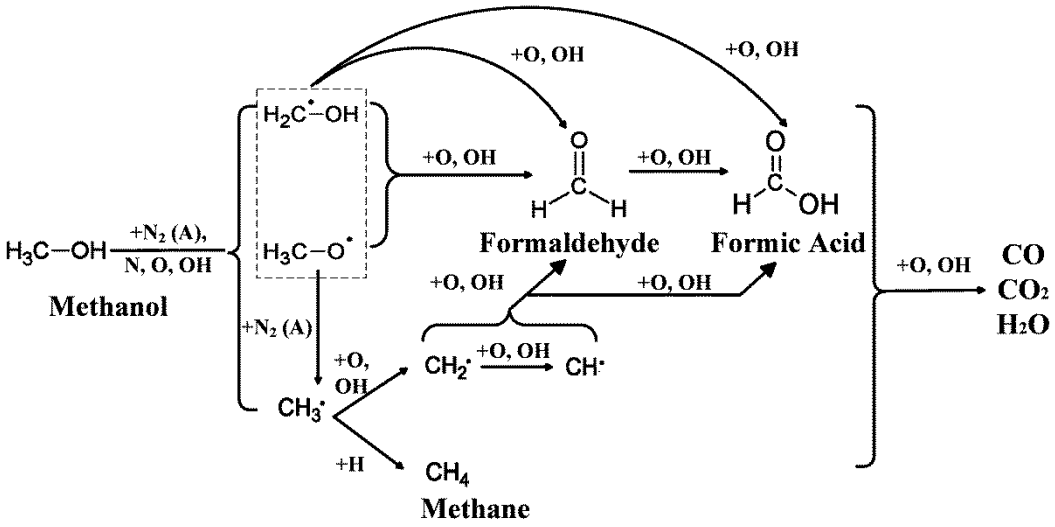

(a)

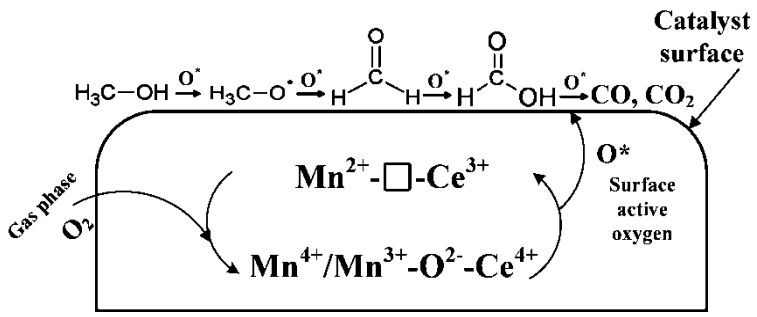

(b)

Fig. 9. Plausible major reaction pathways of methanol removal in the post-plasma catalysis system: (a) Plasma induced chemical reactions in the discharge region; (b) Catalytic reactions on the catalyst surface. The 'square' symbol represents oxygen vacancies on the surface of the Mn-Ce catalysts.

4. Conclusions

In this study, effective removal of methanol over Mn-Ce oxide catalysts with different Mn/Ce molar ratios has been achieved in a post-plasma catalysis system. Compared to pure MnO_x and CeO_2 oxide catalysts, the combination of plasma and binary Mn-Ce catalysts significantly enhances both methanol removal efficiency and energy efficiency of the plasma-catalytic process, while the $Mn_{50}Ce_{50}$ catalysts exhibits the best performance among all the tested catalysts. The presence of these Mn-Ce catalysts in the plasma process also inhibits the formation of various by-products including CH_4, HCHO and HCOOH. Possible reaction pathways have been proposed based on the detected by-products. A well-trained and optimized three layer neural network has been used to get a better understanding of the effect and importance of different processing parameters and catalyst composition on the plasma chemical reaction. Sensitivity analysis shows that catalyst composition (Mn percentage) is the most important factor affecting the removal efficiency of methanol, while the discharge power plays a crucial role in the energy efficiency of the plasma-catalytic process. The good agreements between experimental and predicted results indicate ANN model can be an effective approach for fast and reliable simulation and prediction of the complex plasma-catalytic process.

Supporting Information

Definition of MSE and SDE; Comparison of 5 best combinations of BP algorithms and transfer functions with a hidden layer of 5 neurons (Table S1); MSE as a function of neuron number for the LM-TT configuration (Fig. S1); Comparison between measured removal efficiency T and predicted

data Y (Fig. S2); Weight matrices W1 (weights between the input and hidden layers) and W2 (weights between the hidden and output layer) (Table S2).

Acknowledgements

Support of this work by the UK EPSRC Bioenergy Challenge Programme (EP/M013162/1), National Natural Science Foundation of China (No. 51076140 & No. 51206143) and National Science Fund for Distinguished Young Scholars (No. 51125025) is gratefully acknowledged.

References

[1] J.H. Seinfeld, S.N. Pandis, Atmospheric chemistry and physics: from air pollution to climate change, John Wiley & Sons, 2012.

[2] K.B. Schnelle Jr, C.A. Brown, Air pollution control technology handbook, CRC press2001.

[3] F. Thevenet, L. Sivachandiran, O. Guaitella, C. Barakat, A. Rousseau, J. Phys. D: Appl. Phys. 47 (2014) 224011.

[4] J.C. Whitehead, Pure Appl. Chem. 82 (2010) 1329-1336.

[5] H. Zhang, K. Li, T. Sun, J. Jia, Z. Lou, L. Feng, Chem. Eng. J. 241 (2014) 92-102.

[6] L. Sivachandiran, F. Thevenet, P. Gravejat, A. Rousseau, Chem. Eng. J. 214 (2013) 17-26.

[7] A.M. Harling, D.J. Glover, J.C. Whitehead, K. Zhang, Appl. Catal. B: Environ. 90 (2009) 157-161.

[8] X.B. Zhu, X. Gao, R. Qin, Y.X. Zeng, R.Y. Qu, C.H. Zheng, X. Tu, Appl. Catal. B: Environ. 170 (2015) 293-300.

[9] X. B. Zhu, X. Gao, X. N. Yu, C. H. Zheng, X. Tu, Catal. Today, 256 (2015), 108-114

[10] X. Fan, T.L. Zhu, M.Y. Wang, X.M. Li, Chemosphere, 75 (2009) 1301-1306.

[11] H.Q. Trinh, Y.S. Mok, Chem. Eng. J. 251 (2014) 199-206.

[12] J. Jarrige, P. Vervisch, Appl. Catal. B: Environ. 90 (2009) 74-82.

[13] Y. Li, Z. Fan, J. Shi, Z. Liu, W. Shangguan, Chem. Eng. J. 241 (2014) 251-258.

[14] F. Lin, X. Wu, S. Liu, D. Weng, Y. Huang, Chem. Eng. J. 226 (2013) 105-112.

[15] S.M. Saqer, D.I. Kondarides, X.E. Verykios, Appl. Catal. B: Environ. 103 (2011) 275-286.

[16] D. Delimaris, T. Ioannides, Appl. Catal. B: Environ. 84 (2008) 303-312.

[17] N. Drenchev, I. Spassova, E. Ivanova, M. Khristova, K. Hadjiivanov, Appl. Catal. B: Environ. 138 (2013) 362-372.

[18] M.T.N. Dinh, J.M. Giraudon, A.M. Vandenbroucke, R. Morent, N. De Geyter, J.F. Lamonier, Appl. Catal. B: Environ. 172 (2015) 65-72.

[19] A.M. Vandenbroucke, R. Morent, N. De Geyter, C. Leys, J. Hazard. Mater. 195 (2011) 30-54.

[20] X. Tu, J.C. Whitehead, Appl. Catal. B: Environ. 125 (2012) 439-448.

[21] W. Somers, A. Bogaerts, A.C.T. van Duin, E.C. Neyts, Appl. Cataly. B: Environ.154 (2014) 1-8.

[22] E.C. Neyts, K. Ostrikov, Catal. Today 256 (2015) 23-28.

[23] H. Huang, D. Ye, D.Y.C. Leung, F. Feng, X. Guan, J. Mol. Catal. A: Chem. 336 (2011) 87-93.

[24] A.M. Vandenbroucke, R. Aerts, W. Van Gaens, N. De Geyter, C. Leys, R. Morent, A. Bogaerts, Plasma Chem. Plasma Process. 35 (2014) 217-230.

[25] E.C. Neyts, A. Bogaerts, J. Phys. D: Appl. Phys. 47 (2014) 224010.

[26] R. Aerts, X. Tu, W. Van Gaens, J.C. Whitehead, A. Bogaerts, Environ. Sci. Technol. 47 (2013) 6478-6485.

[27] R. Aerts, X. Tu, C. De Bie, J. C. Whitehead, A. Bogaerts, Plasma Process. Polymers 9 (2012) 994-1000.

[28] I.A. Basheer, M. Hajmeer, J. Microbiol. Meth. 43 (2000) 3-31.

[29] Istadi, N.A.S. Amin, Ind. Eng. Chem. Res. 45 (2006) 6655-6664.

[30] S.Y. Liu, D.H. Mei, Z. Shen, X. Tu, J. Phys. Chem. C 118 (2014) 10686-10693.

[31] T.C. Manley, T. Electrochem. Soc. 84 (1943) 83.

[32] H. Chen, A. Sayari, A. Adnot, F. Larachi, Appl. Catal. B: Environ. 32 (2001) 195-204.

[33] X. Wang, Y. Zheng, Z. Xu, Y. Liu, X. Wang, Catal. Sci. Technol. 4 (2014) 1738-1741.

[34] X. Tang, J. Chen, X. Huang, Y. Xu, W. Shen, Appl. Catal. B: Environ. 81 (2008) 115-121.

[35] G.D. Garson, AI expert, 6 (1991) 46-51.

[36] P.F. Lee, H. Matsui, D.W. Xu, N.S. Wang, J. Phys. Chem. A 117 (2013) 525-534.

[37] S. Hamdane, Y. Rezgui, M. Guemini, Kinet. Catal. 53 (2012) 648-664.

[38] P.G. Kristensen, B. Karll, A.B. Bendtsen, P. Glarborg, K.I.M. Dam-Johansen, Combust. Sci. Technol. 157 (2000) 262-292.

[39] W. Sun, M. Uddi, S.H. Won, T. Ombrello, C. Carter, Y. Ju, Combust. Flame 159 (2012) 221-229.

[40] S. Todorova, A. Naydenov, H. Kolev, J.P. Holgado, G. Ivanov, G. Kadinov, A. Caballero, Appl. Catal. A: Gen. 413-414 (2012) 43-51.

[41] J.P. Durand, S.D. Senanayake, S.L. Suib, D.R. Mullins, J. Phys. Chem. C 114 (2010) 20000-20006.

[42] C. Doornkamp, V. Ponec, J. Mol. Catal. A: Chem. 162 (2000) 19-32.

[43] O. D'Alessandro, H.J. Thomas, J.E. Sambeth, React. Kinet. Mech. Cat. 107 (2012) 295-309.

[44] E. Finocchio, G. Busca, Catal. Today 70 (2001) 213-225.

[45] K.R. Phillips, S.C. Jensen, M. Baron, S.C. Li, C.M. Friend, J. Am. Chem. Soc. 135 (2013) 574-577.

[46] S. Park, Y. Xie, M.J. Weaver, Langmuir, 18 (2002) 5792-5798.